Charge ratio of ultra-high-energy cosmic-ray muons*

G. K. Ashley II,[†][‡] J. W. Keuffel,[§] and M. O. Larson[||]

Physics Department, University of Utah, Salt Lake City, Utah 84112

(Received 18 February 1975)

We describe the data analysis and report the results of the final charge-ratio experiment using the Utah cosmic-ray muon detector. Values for the charge ratio were obtained from least-squares fits to the observed bending-angle distributions. The fitting function was the result of folding the noise scattering distribution into the ideal local-spectrum bending distribution, with the charge ratio as a parameter of the fit. This method permitted a greater precision while circumventing the main causes of charge-ratio dilution. We obtain the average value 1.378 ± 0.015 for muon momentum at production between 1 and 8 TeV/c, corresponding to a median primary cosmic-ray momentum range 8–61 TeV/c. With the results of this experiment the charge ratio is precisely known over about three decades of muon energy beginning around 10 GeV. Thus, we believe the charge ratio can serve as a touchstone in determining the hadronic interaction dynamics and composition of the primary cosmic rays. Already approximate agreement has been obtained with experimental results from predictions utilizing the scaling-limiting-fragmentation hypothesis and constant composition of the primary cosmic rays.

I. INTRODUCTION

A. Motivation

Cosmic ray muons originate from the decay of mesons produced by the interactions of ultra-high-energy cosmic-ray primaries with atmospheric nuclei. These muons reflect the charge of their parent mesons, which are predominantly positive because the primary cosmic-ray flux consists mostly of free protons. Thus the muon charge ratio (defined as the ratio of the number of positive muons to the number of negative muons) will be greater than unity. The precise value, however, depends not only upon the composition of the primary flux, but also the details of the hadronic interaction. Thus, muon charge-ratio measurements provide an experimental constraint on any acceptable combination of models of high-energy hadronic interactions and primary cosmic-ray composition.

B. Previous charge-ratio measurements

An analysis by Thompson[1] of a large number of previous measurements shows that over the muon production energy range 2–1000 GeV the charge ratio is essentially constant and the majority of experiments are statistically compatible. Representative of the near-vertical experiments are the papers by Ayre *et al.*[2] reporting an average value of 1.285 ± 0.002 over the muon energy range 10–450 GeV, by Allkofer *et al.*[3] reporting 1.29 ± 0.02 for muon energies greater than 10 GeV, by Nandi and Sinha[4] reporting 1.28 ± 0.02 at energies greater than 5 GeV. Representing experiments over a range of zenith angles, Burnett *et al.*[5,6] report an average charge ratio of 1.255

± 0.007 for energies greater than 25 GeV. Because of the steeply falling cosmic-ray muon spectrum, however, such average charge ratios are dominated by the observations at low energy.

The momentum of a charged particle is inversely proportional to the magnitude of the angle through which it is deflected by a magnetic induction field. Since a magnetic spectrometer has a smallest resolvable bending angle, there exists a maximum detectable momentum, p_{mdm}. For surface spectrometers, both the sign of the muon charge and the muon momentum are determined simultaneously from a single bending-angle observation (the sign of the charge from the sign of the bending angle and the momentum from its magnitude). As the muon momentum approaches p_{mdm}, the probability that the wrong sign of the muon charge has been determined becomes non-negligible, causing a dilution of the observed charge ratio. Thus, the maximum energy at which surface measurements of the charge ratio can reliably be made is determined by p_{mdm}. However, in practice it is usually determined by the spectrometer aperture not being large enough to compensate for the steeply falling spectrum.

These difficulties are alleviated by measuring the muon charge ratio using an underground magnetic spectrometer of sufficiently large aperture to overcome the steeply falling spectrum. The high-energy muon spectrum is transformed into a low-energy spectrum at the spectrometer site by the energy losses in the overburden. Therefore, the mean muon production energy is decoupled from the magnetic bending and can be determined from the relevant slant depth of rock transversed using suitable muon survival probabilities.[7]

The first precise charge-ratio measurements above 1 TeV were made by Parker[8] using the underground Utah Cosmic-Ray Muon Detector. He reports an average value 1.306 ± 0.034 over the zenith angle range $40-80°$ for mean production energies 1–10 TeV. This value is about 5% low because of remaining dilution of the kind previously described. Nonetheless, Parker's results show that the charge ratio does not fall to unity for energies in the range 1–4 TeV. Considering the surface measurements it appears to remain fairly constant from 2 GeV to 7 TeV, notwithstanding the low value reported by Parker at 7 TeV resulting from a systematic error. This error will be discussed in Sec. II C.

C. Present experiment

To corroborate Parker's results, a second charge-ratio experiment was conducted at Utah, using the same experimental apparatus and data gathering procedures. However, a unique method of analysis was used wherein the charge ratio is treated as an unknown parameter in the otherwise known local muon spectrum. Its value is obtained by a least-squares fit of the bilateral convolution of this local spectrum and the detector bending-angle resolution function to observed muon bending-angle distributions. The resulting values cover the mean muon production energy range 1–8 TeV corresponding to a median primary energy range 8–61 TeV, the lower limit of which is four times greater than the maximum equivalent laboratory energy currently available at the CERN colliding-beam accelerator. Parker's data, when reanalyzed using this new method, yield results which are found to be totally consistent with those of this experiment. Therefore, Parker's raw data is combined with ours, and analyzed by the above procedure to obtain more precise values for the charge ratio. The results of an early analysis have already been reported.[9,10]

II. EXPERIMENTAL PROCEDURE

A. Apparatus

The University of Utah underground cosmic-ray detector has now been in operation for several years, and has been described in some detail.[11-14] For orientation purposes a brief description of the detector components germane to this experiment will be given here (see Fig. 1).

Each of the two detector magnets consists of seven vertical legs which are 60.3 cm thick, have an effective height of 5.0 m, and are 1.2 m long, except for the end legs which are 0.6 m long. The magnetic field in each leg is 16.3 ± 0.8 kG, and the

resulting stored energy in both magnets is 145 kJ. Because of joule losses in the magnet coils it is necessary to expend 13.4 kW to maintain the magnetic field. The flux path is closed at the top and bottom of the magnet legs by "keepers." Thus the magnetic induction is alternately up and down in the legs. This alternation provides a first-order cancelation of systematic errors present in the charge-ratio experiment.

The cylindrical spark counters are steel pipes 15.24 cm in diameter and have an acoustical length of about 10 m. They are filled with 67% argon and 33% ethylene to a pressure of 750 mm of Hg at 20 °C. Along the axis of each spark counter is stretched a wire on which a 6-kV clearing potential is maintained with respect to the counter wall. When the Cherenkov system triggers the detector, the center wire potential is raised to 8.4 kV for 2 μsec. Thus, the spark counters resemble oversized Geiger counters operated in a pulsed mode and at a higher pressure so that the discharge is a sharply localized corona spike. The principal acoustic mode excited by this spark discharge is a plane wave which propagates along the spark counter axis. In a 15-cm pipe, modes other than the principal one have attenuation lengths of about 1 m or less for frequencies below 3 kHz, while the attenuation of the principal mode is about 50% over 10 m. The position of the spark along the counter axis (y coordinate) is determined by measuring the time delay between the triggering of the detector and the arrival of the sound at a microphone located at the front ($y = 0$) of the counter. The precision of localization of a spark is about 3 mm, and two sparks separated by 10 cm can be resolved. The spark-counter column (x coordinate) and the height (z coordinate) are obtained from previous survey measurements to the counter center wires. The position of each spark is digitized and recorded on magnetic tape for later computer analysis. It should be noted that multiple-track ambiguities inherent in crossed wire-chamber or flash-tube systems are absent—a circumstance of great importance especially in the automatic pattern recognition programs, when a number of tracks are present.

B. Collection of data

In the absence of scattering and instrumental errors, the projection of a muon trajectory onto the xy plane of the detector is a straight line, a circular arc through a magnet leg, and another straight line, which we represent by the equation

$$y = \theta(-x)a_1 x + \theta(x)a_2 + b , \qquad (1)$$

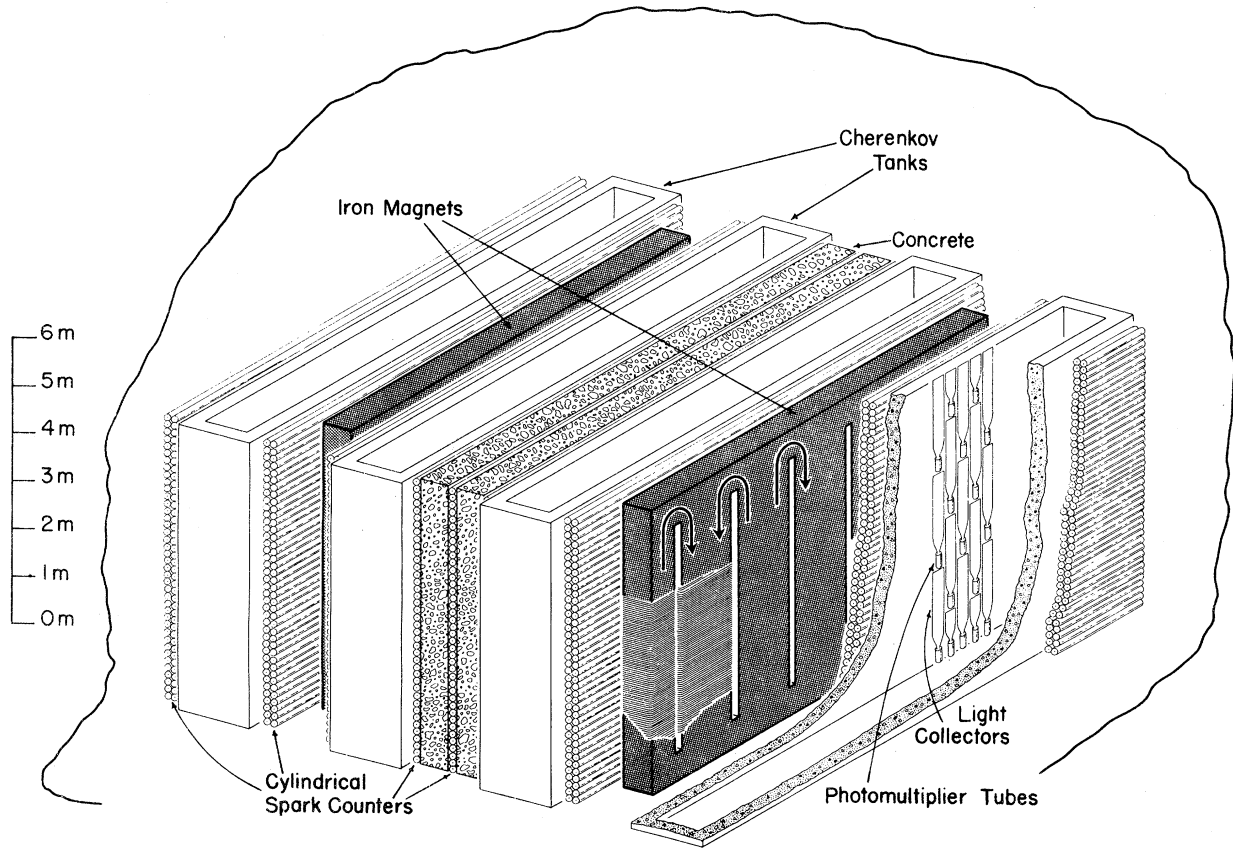where $\theta(x)$ is the unit step function, and the line

FIG. 1. The Utah cosmic-ray muon detector (viewed from the front) is located beneath the Wasatch Mountains at Park City, Utah. For the charge-ratio experiment it accepts muons with zenith angles between 40° and 90° corresponding to slant depths in excess of 2×10^5 g cm^{-2}. The detector consists of 600 cylindrical spark counters arrayed in 15 vertical planes, each 6 by 11 m, two vertical planes of concrete absorber (SiO$_2$), each 6 by 10 m and 122 cm thick, four water Cherenkov counters which trigger the detector, each housed in a concrete tank with 30-cm walls, and two vertical iron magnets, each containing 7 legs 60 cm thick with a magnetic field of 16.3 ± 0.8 kG.

$x = 0$ is taken to coincide with the centerline of the traversed magnet leg. Equation (1) only applies outside the magnet. A trajectory with greatly exaggerated bending is shown in Fig. 2. Parameters a_1, a_2, and b are determined by fitting Eq. (1) to the spark coordinate pairs (x_i, y_i) using the method of least-squares. The observed muon bending angle is then defined to be

$$\alpha = s |\tan^{-1}(a_1) - \tan^{-1}(a_2)| . \qquad (2)$$

The factor $s = \pm 1$ is assigned for each muon event according to the known direction of travel through the detector and the orientation of the magnetic field in the traversed magnet leg. Thus, if a *positive* muon were to undergo a *magnetic* deflection in the same direction and under the same conditions as the muon being considered, then $s = +1$; otherwise, $s = -1$.
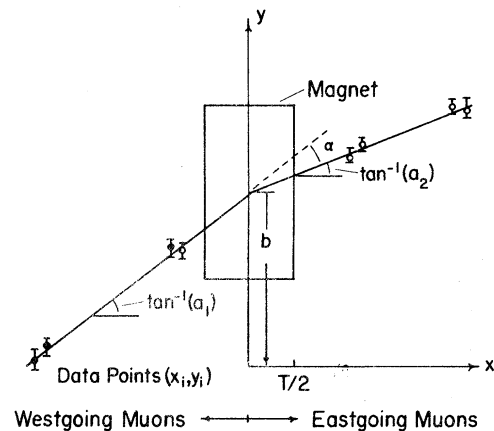

FIG. 2. Projection of a muon trajectory through a magnet leg onto the xy plane. The actual path in the leg is circular. The straight lines shown are given by Eq. (1).

In general the intersection of the two straight-line portions of the muon trajectory is not along the centerline of the traversed magnet leg. Therefore, Eq. (2) underestimates the true bending angle by an amount that is dependent upon the muon azimuth angle ϕ (defined as the angle the muon trajectory makes with the xz plane before entering the magnet leg). This discrepancy has a maximum value of 10%, and since most muons have an azimuth angle less than 25°, the discrepancy is generally less than 1%.

All muons incident upon the Utah detector which traverse *both* yz faces of a magnet leg and have a lever arm defined by sparks on both sides of the leg are accepted for the determination of the charge ratio. These accepted muons make up about 40% of the total number of eligible muons. The accepted muons are grouped according to their zenith angle θ and slant depth h of rock through which they passed. These groupings, or "bins," are 10° in zenith angle by 10^5 g cm^{-2} in slant depth, and range over 40° to 90° in zenith angle and from 2×10^5 g cm^{-2} to 8×10^5 g cm^{-2} in slant depth. Muons in a particular bin are formed into a discrete distribution of observed bending angles according to

$H(\alpha_i)$=number of muons with $\alpha_i - 1 < \alpha < \alpha_i + 1$ mrad,

where   (3)

$$\alpha_i = 2(i - 25.5) \text{ mrad } (i = 1, 2, \ldots, 50).$$

Each bin is then assigned a mean zenith angle θ, azimuth angle ϕ, and slant depth h, which are obtained from the averages of the respective quantities of the bin's constituent muons. The ranges of the individual zenith angles and slant depths are restricted by the size of a bin, and the majority of azimuth angles are clustered about an average value.

Thus, the data for this experiment consists of the bending angles α for accepted muons, grouped according to zenith angle and slant depth.

C. Corrections to the data

The corrections made to the data fall into two categories: (1) corrections made to individual muon trajectories, and (2) corrections made to individual bending angles. Corrections of the first kind are made to achieve optimum precision in spark position and consist of principal plane, knock-on electron, and oblique muon corrections. Corrections of the second kind are made to eliminate any systematic bending-angle error common to the muons of a particular bin.

Principal plane correction. The discharge of a cylindrical spark counter occurs at that point where the muon passes closest to the spark-counter wire. This point is determined by the biperpendicular to both the center wire and the muon trajectory. Because of the large spark-counter diameter, muons can pass through the counter sensitive volume up to 7.4 cm from the center wire and still discharge the counter [Fig. 3(a)]. Consequently, when the trajectory is projected onto the xy plane, the sparks in general will not fall along the projected trajectory [Fig. 3(b)], even in the ideal case where all other considerations vanish. Rather, they will have deviations in the y direction between 0 and 8.0 cm.

This effect is eliminated if the trajectory were to be projected instead onto the "principal plane," defined as that plane containing the muon trajectory and parallel with the y axis. However, we choose to proceed in the equivalent manner in the xy plane by adjusting the x coordinates of each spark to compensate for this geometrical effect. To do this, we first make a linear fit to the trajectory projected on the xz plane where there is no magnetic bending. Next, the projected zenith angle θ_p and the deviations d_i in the z direction of the sparks from the linear fit are determined. The correction is then made by adding the quantity $\frac{1}{2} d_i \sin(2\theta_p)$ to the spark coordinates x_i.
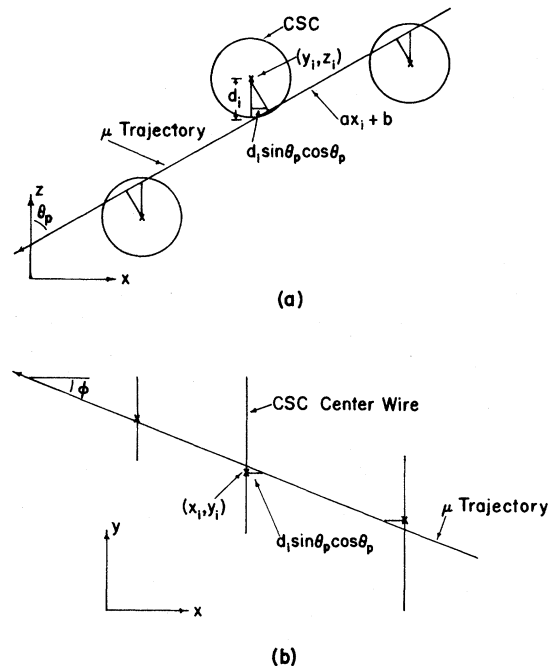
The limiting factor in the accuracy of the

(a)

(b)

FIG. 3. Examples of a muon trajectory and cylindrical spark counter (CSC) discharges (not to scale) projected onto (a) the xz plane, and (b) the xy plane.

principal-plane correction is ultimately the un-
certainty in the linear fit to the trajectory in the
xz plane. Both x_i and z_i are known to within
± 0.159 cm from survey measurements. The
error in θ_p is thus computed to be less than ± 0.32
mrad. Therefore, the errors in the "new" x co-
ordinates lie between ± 0.159 and ± 0.263 cm.

Knock-on electron correction. In traversing a
cylindrical spark counter, a muon produces knock-
on electrons in the counter wall. It is then possi-
ble for these electrons also to discharge the spark
counter. From the differential collision probabil-
ity for producing a knock-on electron by particles
of spin $\frac{1}{2}$,[15] and the relation between the kinetic
energy and opening angle of the produced elec-
tron,[16] it is apparent that the production probabil-
ity increases with increasing opening angle, and
has azimuthal symmetry. However, because of
the cylindrical nature of the spark counters, the
probability for a knock-on electron to discharge a
counter at distances greater than a specified
amount from the point of closest approach of the
muon to the spark-counter center wire decreases
as this specified distance increases.

The deviations of sparks about a mean value is
the superposition of a narrow distribution due to
the muon discharges plus a much broader distri-
bution resulting from the knock-on electrons.
Fitting a Gaussian curve to the central portion
of the total distribution yields an rms value of
about 0.5 cm. It is obvious that the "wings" of
this distribution, which are due mainly to knock-
on electrons, will have an undesirable effect upon
the least-squares fit to the projection of the muon
trajectory onto the xy plane. Therefore, we want
to eliminate as many knock-on electron sparks as
possible without eliminating any muon sparks.
This we do by making a "cut" at about 1.5 cm on
the deviations of sparks from the computed tra-
jectory in the xy plane, and regard those with
greater deviations as arising from knock-on elec-
trons. Although the choice for the cut at 1.5 cm
was arbitrary, we feel that placing it at three
standard deviations of the assumed muon spark
distribution was sufficient.

To reduce the influence of the knock-on elec-
trons, we proceeded in the following manner.
After Eq. (1) had been fitted to the initial set of
sparks for a given event, those which were con-
sidered to be due to knock-on electrons were neg-
lected. The remaining sparks were then again
fitted by Eq. (1), and the resulting deviations
tested for knock-on electrons. This procedure
continued until one of three situations occured:
(1) $\frac{1}{2}$ of the original number of sparks had been
neglected, in which case the event was considered
ambiguous and rejected, (2) sufficient sparks had
been removed such that it was no longer possible
to define one or both of the trajectory lever arms,
or (3) all remaining sparks had deviations less
than about 1.5 cm and the event was accepted for
further analysis.

Oblique muon correction. Between the time the
detector is triggered and the spark counters reach
full operating voltage, some of the ionized elec-
trons in the counters will be collected by the clear-
ing potential if the muon passed close enough to
the spark-counter center wire. When the counter
attains full operating voltage, two separated
strings of electrons then exist, and two corona-
spike discharges then occur for oblique muons.
The distance between the discharges is a function
of the distance of the trajectory from the center
wire and the angle of obliquity. The angle of obli-
quity is defined as the angle between the muon
path and the spark-counter center wire in the
principal plane.

An anomaly of the cylindrical spark-counter
electronics is that following its response to an
acoustic pulse an undershoot occurs, creating a
trough of approximately the same magnitude and
width as the acoustic pulse. If the separation of
the two discharges of an oblique muon is between
about 6.2 and 12.4 cm, the second acoustic pulse,
originating from the discharge furthest from the
counter microphone, will be in this trough and
may not be detected. At angles of obliquity less
than 45°, this second pulse will be on the first
pulse side of the trough. It will combine with the
first pulse, with the result that the y coordinate
of the spark nearest the counter microphone will
be displaced toward the "correct" spark position.
This "correct" spark position would be the one
observed in the absence of these effects, and has
a y coordinate equal to the mean of the y coordi-
nates of the two discharges. The symmetry of the
discharges is thus destroyed with a pronounced
effect upon the accuracy of the least-squares fit
to the muon trajectory.

Using the results of experiments conducted by
Wilson[17] to study this phenomenon, we developed
an empirical correction to neutralize the effect
the masking of the second pulse has on the muon
trajectory. This correction depends upon the
angle of obliquity and the distance of the trajec-
tory from the center wire. For angles of obliquity
less than about 20°, the correction is less than
the 10 μsec resolution (~ 0.156 cm) of the elec-
tronics and was not applied. Owing to the ter-
rain above the detector, the slant depth is a func-
tion of muon zenith and azimuthal angles. Only
for those muons with zenith angles and slant
depths in excess of 75° and 6×10^5 g cm^{-2} were
the zenith and azimuth angles such that the angle

of obliquity was of sufficient magnitude to warrant applying the correction.

For each event with zenith angle and slant depth greater than the above values, all double sparks were checked to see if their separation agreed with the expected separation. Those that did agree within a specified tolerance were regarded as true double sparks. In the determination of the muon trajectory they were replaced with one spark with a y coordinate equal to the average of the y coordinates of the two sparks. Those double sparks that did not agree with the expected separation were considered to be a single spark produced by a muon and a spark produced by a knock-on electron. That spark which was closest to the computed muon trajectory was chosen as the muon-produced spark. All singly occuring sparks were considered double sparks with the second spark completely masked. The above empirical correction for masking was applied. This correction was of the order of 1.3 cm. Failure to apply the oblique muon correction led to a dilution of the observed value for the charge ratio by Parker[8] in this same slant depth and zenith angle range.

Systematic bending-angle error correction. In the Utah detector a systematic bending-angle error α_s was observed due to a systematic displacement of the y coordinates of sparks in the cylindrical spark counters adjacent to the magnets. The longitudinal temperature gradients along the spark counters near the magnets are the principal cause of these displacements. These temperature gradients are produced by heat from Joule losses in the magnet field coils. Therefore, it is not possible to determine α_s by reducing the magnetic field to zero and measuring a mean bending-angle, since this would change the temperature gradients and α_s. However, it is possible to accurately determine α_s by utilizing the symmetry of the detector.

The Utah detector can be thought of as a collection of 14 separate magnetic spectrometers—one for each magnet leg. A muon can traverse a magnet leg in one of two possible "directions" which correspond to whether the projection of the muon's motion along the x axis is in the $+x$ or $-x$ direction. Constituent muons of a particular slant depth–zenith angle bin are separated into four groups according to muon "direction" and the orientation of the magnetic field in the traversed magnet leg. Each group of muons forms a bending-angle histogram analogous to that generated by Eq. (3). Consider two such histograms consisting of muons traversing magnet legs in one specified "direction" with the magnetic field parallel to the z axis for one histogram and antiparallel to the z axis for the other. In the absence

of any systematic bending-angle error, these two histograms would be in coincidence; and their mean bending angles equal to the true mean bending angle α_m which is a function of the charge ratio. Because of the definition of the sign of the bending angle α in Eq. (2), the sign of α_s will necessarily change if the magnetic field for a given muon "direction" were to be reversed. Thus, for a nonzero α_s the two histograms will be translated in opposite directions from α_m by the magnitude of α_s. These translated histograms are then what is observed. The value of α_m is obtained from the arithmatic average of the mean bending angles of the two translated histograms. For the two histograms which correspond to the other muon "direction," α_m is similarly determined. The resulting values for each direction are found to be statistically consistent. A weighted average for α_m is determined from the values for each direction. Each of the four histograms is translated by the difference between its mean bending angle and the average α_m, such that all four histograms will coincide. The systematic bending-angle error is thus corrected for, and a new total histogram is formed by a sum of the four corrected histograms.

Muons passing through similar parts of the detector will have a similar systematic error in bending angle. Therefore, the correction for α_s is applied separately to each of the bins. For all data used in this experiment, the magnitude of α_s was found to have an average value $(2.807 \pm 0.344) \times 10^{-4}$ rad, and ranged from 8.89×10^{-5} to 5.81×10^{-3} rad.

We point out that in terms of size this correction is of second order. A first-order cancellation of any systematic bending-angle error is provided by the alternating magnetic field in adjacent magnet legs. This is augmented by periodically reversing the current direction in the magnet field coils to guarantee that equal numbers of muons for a given direction will traverse both orientations of the magnetic field.

III. CHARGE-RATIO ANALYSIS

A. Outline of method

Once the corrected bending-angle histograms have been determined, we can proceed to obtain from them values for the charge ratio corresponding to particular bins of slant depth and zenith angle. To do this we need to know the vertical depth-intensity spectrum of muons from which we obtain the local energy spectrum at the detector. The local energy spectrum consists of positive and negative muons in the ratio R. This local

spectrum is transformed into the ideal bending-angle spectrum where the charge ratio appears explicitly as an unknown free parameter. When convoluted with the known bending-angle resolution function, the ideal bending-angle spectrum yields a predicted distribution of bending angles. This is integrated to form a histogram which is fitted by the method of least-squares to an observed bending-angle histogram to obtain the charge ratio. The success of this method depends upon knowledge of the local muon spectrum, how it is transformed to the ideal bending-angle spectrum, and upon knowledge of the bending-angle resolution function for the detector.

B. Local energy spectrum

The local differential energy spectrum $m(E)$ for muons incident upon the Utah detector is obtained from the integral depth-intensity spectrum, and the rate of energy loss of muons in rock. An empirical fit to a world survey of vertical depth-intensity data by Groom[18] yields

$$I_v(x) = I_1 \exp(-x/\lambda_1) + I_2 \exp(-x/\lambda_2), \quad (4)$$

where $\lambda_1 = 3.66 \times 10^4$ g cm^{-2}, $\lambda_2 = 7.95 \times 10^4$ g cm^{-2}, $I_1 = 12.8 \times 10^{-6}$ sec^{-1} cm^{-2} sr^{-1}, and $I_2 = 1.3 \times 10^{-6}$ sec^{-1} cm^{-2} sr^{-1}. The depth-intensity spectrum at zenith angle θ is obtained by multiplying Eq. (4) by the atmospheric enhancement function $G(x, \theta)$. Thus, $I(x, \theta) = I_v(x)G(x, \theta)$, where $G(x, \theta)$ has very little depth dependence and varies approximately as the secant of the zenith angle of the muon trajector at production.

We assume a rate of muon energy loss in standard rock of the form

$$-dE/dx = [a(E) + b(E)E] \text{ GeV/g cm}^{-2}, \quad (5)$$

where $a(E)$ represents the energy loss due to ionization, and $b(E)$ represents the energy less due to the catastrophic energy losses: bremsstrahlung, pair production, and nuclear interactions. Since $a(E)$ and $b(E)E$ are equal at about 630 GeV,[19] we can assume $b(E)$ to be continuous with little effect upon the local energy spectrum. Therefore, a muon at a slant depth h with energy E will have a *total* slant depth

$$x(E) = h + \int_0^E [a(E) + b(E)E]^{-1} dE. \quad (6)$$

From the conservation of particles, the number of muons $m(E)dE$ at slant depth h and the zenith angle θ with energy near E in dE will be equal to the number which stop at a slant depth x in dx. Consequently, the local energy spectrum is given by

$$m(E)dE = -[a(E) + b(E)E]^{-1}$$

$$\times \frac{d}{dx} I(x, \theta)dE \text{ sec}^{-1} \text{ cm}^{-2} \text{ sr}^{-1}, \quad (7)$$

where the derivative of $I(x, \theta)$ is to be evaluated at the slant depth given by Eq. (6).

C. Ideal bending - angle spectrum

The magnetic bending angle α_B is related to the energy E of a muon traversing the Utah detector via $\alpha_B = K/E$ when $K = 0.295 \csc\theta \sec\phi$ GeV. Using the sign convention of Eq. (2) will guarantee that $\alpha_B > 0$ for positive muons, and $\alpha_B < 0$ for negative muons. The ideal bending-angle spectrum $j(\alpha_B, R)$ is defined as the resulting distribution in magnetic bending angle from muons incident upon the detector in the absence of any scattering and measurement errors. It is given by

$$j(\alpha_B, R)d\alpha_B = d\alpha_B \int_{E_0}^{+\infty} m(E)\left[\frac{R}{R+1} \delta\left(\alpha_B - \frac{K}{E}\right) + \frac{1}{R+1} \delta\left(\alpha_B + \frac{K}{E}\right)\right] dE \text{ sec}^{-1} \text{ cm}^{-2} \text{ sr}^{-1}, \quad (8)$$

where $E_0 = 2.42 \csc\theta \sec\phi$ GeV is the minimum muon energy necessary to traverse one magnet leg and sufficient spark counters to determine the trajectory, δ is the Dirac δ function, and R is the charge ratio of the incident muons. Empirically, the dependence of R upon E is rather weak, and since $m(E)$ falls steeply with increasing E we can safely take R to be constant and integrate to $+\infty$ in Eq. (8). A plot of $j(\alpha_B, R)$ is given in Fig. 4.

D. Bending - angle resolution function

The probability for a muon which has traversed a magnet leg and acquired a *magnetic* bending angle α_B to have an *observed* bending angle near α in $d\alpha$ is defined as the bending-angle resolution function. The measurement errors responsible for this resolution function are mainly due to the random fluctuations in the parameters a_1 and a_2 of Eq. (1) and to Coulomb scattering. Approxi-

mately 80% of the Coulomb scattering suffered by muons passing through the detector occurs in the magnet legs. Because the ratio of α_B to the xy projection of the root-mean-square Coulomb scattering angle for a magnet leg is greater than 3.4, Coulomb scattering is assumed not to contribute significantly to the resolution function. The bending-angle resolution function is thus written $B(\alpha - \alpha_B, w)d\alpha$. It depends on muon energy only through α_B and is symmetric about $\alpha = \alpha_B$. The parameter w governs the relative width of the resolution function for the various zenith angle–slant depth bins, and has a value near unity. If the bending-angle resolution function is known, the predicted bending-angle distribution of muons for a particular bin is given by

$$F(\alpha, R, w)d\alpha = d\alpha A \int_{-\infty}^{+\infty} j(\alpha_B, R) B(\alpha - \alpha_B, s)d\alpha_B .$$
(9)

The constant A, when multiplied by the number of muons $\sec^{-1}$ cm^{-2} sr^{-1} with energy greater than E_0 obtained from Eq. (7), gives the number of observed muons in that bin. Physically, A represents an average of the product of the detector live time, the efficiency of muon detection, and the aperture for the bin under consideration.

To evaluate $B(\alpha - \alpha_B, w)$ empirically we have used the concrete absorber at the center of the detector. Those muons traversing the concrete absorber are analyzed in the same manner as those traversing the iron magnets. However, the systematic bending-angle error correction is not applied. These muons are also grouped into zenith angle–slant depth bins of the same range with bending-angle histograms defined by Eq. (3). Because the aperture for the concrete absorber is small compared to that for the iron magnets, the number of muons obtained is relatively small. It turns out that there is only one bending-angle
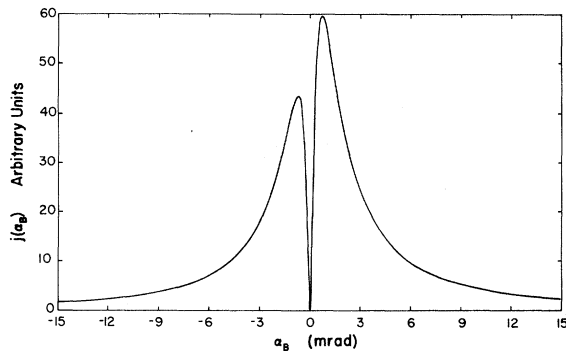

FIG. 4. Ideal bending-angle spectrum $j(\alpha_B, R)$.

histogram $H_a(\alpha_i)$ for the concrete absorber which has enough muons to be well defined over the entire range of α_i. The concrete absorber can be though of as a "magnet" with zero magnetic field. We obtain the expected bending-angle distribution $F_a(\alpha)$ corresponding to $H_a(\alpha_i)$ from Eq. (9) where $j(\alpha_B, R)$ from Eq. (8) is modified by setting $K = 0$:

$$F_a(\alpha)d\alpha = d\alpha A_a B_a(\alpha) \int_{E_0}^{+\infty} m(E)dE$$

$$= N_a B_a(\alpha)d\alpha ,$$
(10)

where N_a is approximately the number of muons in that bin. To relate $F_a(\alpha)d\alpha$ to $H_a(\alpha_i)$, we form the integral sum

$$I_a(\alpha_l) = \sum_{i=1}^{l} H_a(\alpha_i) .$$

$I_a(\alpha_l)$ is then smoothed, made continuous by interpolation, differentiated, and set equal to $F_a(\alpha)$. The smoothing is required to reduce the effect of the satistical fluctuations. $F_a(\alpha)$ is then translated in α so it is symmetric about $\alpha = 0$. This centering removes any systematic bending-angle error. The bending-angle resolution function for the concrete absorber then results from Eq. (10). Because of the similar geometrical relationship between the concrete absorber and the iron magnets with the surrounding cylindrical spark counters, we assume the connection between their bending-angle resolution functions to be given by

$$B(\alpha, w) = w B_a(w \alpha) .$$
(11)

Changing w changes the width of $B(\alpha, w)$ but preserves its shape and normalization. $B_a(\alpha)$ is shown in Fig. 5, and has a value for the dispersion of α equal to 7.952 mrad which corresponds to $37 \csc\theta \sec\phi$ GeV.

Further justification for Eq. (11) will be given later. However, to see if we are on the right track, we make use of a certain class of muons that have traversed both iron magnets. Those two-magnet events with bending-angle magnitudes greater than some cutoff α_c are classified according to whether the signs of their charges were found to be consistent or inconsistent in both magnets. Equation (11) can be used in conjunction with Eq. (8) and assumed values for R (~ 1.38) and w (~ 1.0) to predict the ratio of the number of inconsistent to consistent two-magnet events as a function of α_c. It is obvious that this ratio will decrease with increasing α_c.

The agreement with observation is seen from Fig. 6 to be good to about 14 mrad. Beyond this value, the observed ratio is flat while the prediction falls slowly to zero, and it is empirically ob-
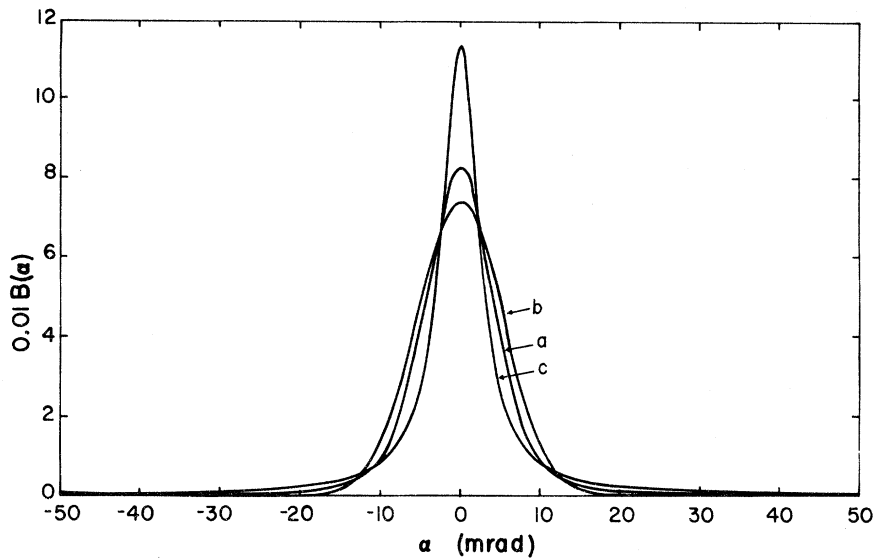
FIG. 5. Bending-angle resolution functions normalized to unity. Curve a is the concrete absorber resolution function $B_a(\alpha)$ with the dispersion in α equal to 7.952 mrad. Curve b is a Gaussian distribution with a root-mean-square deviation equal to 5.4 ± 0.1 mrad. Curve c is Lorentzian or Cauchy distribution with a half width at half maximum equal to 2.8 ± 0.1 mrad.

served that agreement here depends strongly upon the shape of $B(\alpha, w)$ in the regions where the magnitude of α is greater than about 20 mrad. We will later observe that the determination of the charge ratio is insensitive to this region. Therefore, the agreement obtained for the two-magnet events is taken as an indication that the assumptions leading to Eq. (11) were appropriate.

E. Determination of the charge ratio

Normally, each observed bending-angle histogram $H(\alpha_i)$ consists of 50 intervals of α, each 2 mrad wide and centered at each of the α_i defined in Eq. (3). We require that each interval contain at least 10 muons so the Poisson statistics can be approximated with a normal error distribution. If there are less than 10 muons in any interval, adjacent intervals are combined to acquire the required 10 muons. This adjusting of intervals was necessary for 6 of the 10 bins where either detector aperture or large slant depths were responsible for fewer muons. In every bin, however, there were sufficient muons such that each histogram was well defined.

After a bending-angle resolution function has been selected and the above check made on the observed bending-angle histograms, we proceed via the method of least-squares, using Eq. (9) to determine the charge ratio for each of the 10 zenith angle-slant depth bins. First, we integrate

$F(\alpha, R, w)$ over the appropriate intervals of α to construct an expected bending-angle histogram. These intervals are chosen to correspond with those of the observed histogram. Second, we
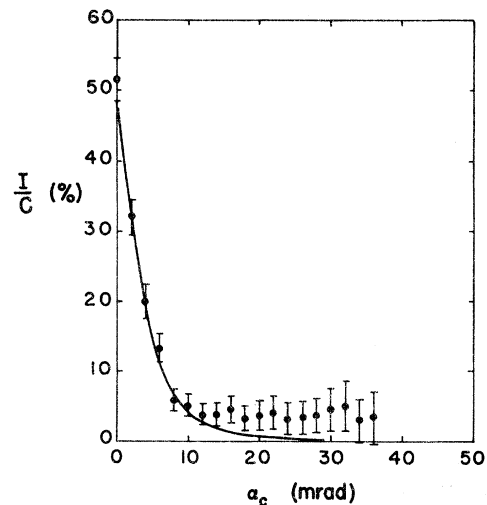

FIG. 6. Two-magnet test. For those muons traversing both magnets with $|\alpha| > \alpha_c$ in each, I/C is the ratio of the number I which have inconsistent determined signs of charge to the number C which have consistent signs of charge.

form the χ^2 of the two histograms:

$$\chi^2(R,w) = \sum_{i=1}^{n} \left[H(\alpha_i) - \int_{\alpha_i - \Delta\alpha_i}^{\alpha_i + \Delta\alpha_i} F(\alpha,R,w)d\alpha \right]^2 \Big/ H(\alpha_i),$$

(12)

where n is the number of bending-angle intervals, α_i are the interval centers, and $\Delta\alpha_i$ are the interval half-widths. Next, we search along the χ^2 surface for the minimum value $\chi^2(R_0,w_0)$. R_0 then represents the "best" value for the charge ratio for the bin being considered. In Fig. 7 we plot $F(\alpha,R_0 w_0)$ along with $H(\alpha_i)$ for bin 2 (see Table I).

Because our least-squares fitting procedure involves searching along the χ^2 surface rather than an analytical solution, there is no analytical expression for the uncertainties in R_0 and w_0. In the limit of a parabolic expansion of the χ^2 surface it can be shown[20] that if we change one parameter by an amount equal to its uncertainty and optimize the other parameter for minimum χ^2, then the new value of χ^2 will be 1 greater than the old value. In this manner we compute the uncertainties in R_0 and w_0.

F. Average muon energy at production

At this point we have determined the "best" value of the charge ratio for each of the 10 zenith angle–slant depth bins. We now associate an average muon energy at production $E_\mu(h,\theta)$ with each bin. Using the survival probabilities $S(E,h)$ calculated by Carlson[7] (defined as the probability that a muon with energy E at production will reach

a slant depth h) and the surface differential energy spectrum $\mu(E,\theta)$, $E_\mu(h,\theta)$ is given by

$$E_\mu(h,\theta) = \frac{(\partial/\partial h)\int_0^\infty E_\mu(E,\theta)S(E,h)dE}{(\partial/\partial h)\int_0^\infty \mu(E,\theta)S(E,h)dE}.$$

(13)

This energy is for stopping muons and therefore is an average threshold energy. Our least-squares, charge-ratio analysis makes use of all muons in a given bin, each with a local energy in excess of about 2.5 GeV. One can ask: What residual energy should be added to $E_\mu(h,\theta)$ to account for the fact our muons did not have zero energy? Consider those incident muons with a local energy in excess of about 50 GeV. For these muons the bending-angle resolution function will always be centered about a point within 6 mrad of the origin. Because of the large width of $B(\alpha - \alpha_B, w)$ relative to that of $j(\alpha_B, R)$, $F(\alpha,R,w)$ will be practically symmetric about zero for small α, and therefore, almost independent of R. Thus, the determination of the charge ratio is insensitive to muons with local energies greater than 50 GeV—rather it depends upon those muons which are near the end of their range. For muons with local energies less than 50 GeV, the mean local energy is about 23 GeV. This is only 3% of the average muon threshold energy for the minimum slant depth of the detector and is neglected. Therefore, the muon energy we assign to the charge ratio of each bin with average slant depth h and zenith angle θ is just $E_\mu(h,\theta)$ with no residual addition.

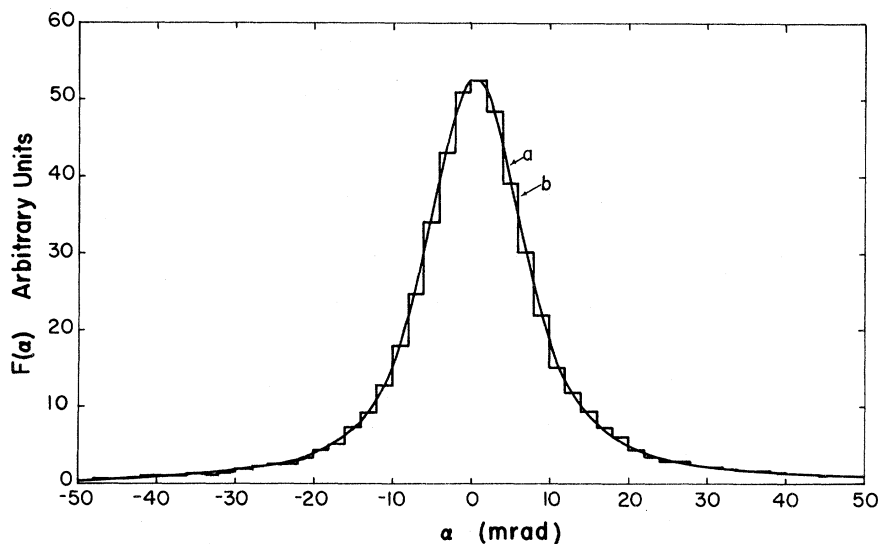It should be noted that the magnets were not used to differentiate between muon energies while

FIG. 7. Curve a: expected bending-angle distribution $F(\alpha,R,w)$; and curve b: observed bending-angle histogram $H(\alpha_i)$; both normalized to unity for bin 2.

simultaneously determining the signs of the muon charges. The energy was determined independently from the magnets by the amount of rock the muon traversed reaching the detector. This avoids running afoul of problems with the maximum detectable momentum of the magnets.

IV. RESULTS OF THE LEAST-SQUARES ANALYSIS

In Table I we present the results of our least-squares fitting procedure for determining the charge ratio. This involved the analysis of 126 122 muons, collected during 765 days of detector live time. They include the 7482 muons used by Parker[8] in his charge-ratio determination. The standard deviations for R_0 and w_0 are the statistical uncertainties in these parameters from the least-squares fits.

Our results indicate that between about 1 and 7.5 TeV the average value for the charge ratio is 1.378 ± 0.015. They are not statistically compatible with the charge ratio falling to unity in this energy range. The dependence of the charge ratio upon muon energy, although not well determined, is consistent with the general rate of increase between 10 GeV and 8 TeV. Because there appears to be no zenith-angle dependence in our charge-ratio values to the order of precision in Table I, we statistically combine those bins with average muon production energies that are close together, viz. bins 1 and 2, 3 and 4, 5 and 6, and 7 and 8. The results are listed in Table II and shown in Fig. 8.

The concrete absorber bending-angle resolution function $B_a(\alpha)$ is equal to $\frac{1}{2}$ its maximum value at ± 5.1 mrad. From Eq. (11) it is apparent that the ratio of the half width at half maximum of the magnet bending-angle resolution function $B(\alpha, w_0)$ to that of $B_a(\alpha)$ is w_0^{-1}. Thus, the results for w_0 from Table I show that for bins 1 through 8, the

$B(\alpha, w_0)$ are slightly wider than $B_a(\alpha)$. We expect $B(\alpha, w_0)$ to be wider than $B_a(\alpha)$ because of the increased importance of Coulomb scattering in the magnets compared to that in the concrete absorber. The fact that it is only slightly wider supports our assumption that Coulomb scattering is unimportant compared to the influence of the rms spark deviations in the spark counters. For bins 9 and 10, $B(\alpha, w_0)$ is about 1.7 times as wide as $B_a(\alpha)$. This is most certainly due to the fact that muons in bins 9 and 10 result from a zenith-angle consolidation for the respective ranges of slant depth before the charge-ratio analysis was done.

Formerly, the method for determining the charge ratio at Utah was to divide the number of observed positive muons with $\alpha > \alpha_c$ by the number of observed negative muons with $\alpha < \alpha_c$, where α_c is some cutoff angle. Because of the width of $B(\alpha - \alpha_B, w)$, some muons incident upon the detector will have the wrong sign of charge determined. As a result the determined value of the charge ratio will suffer dilution, depending upon value of α_c. From Fig. 6 we see that as α_c is increased, the dilution will become small, and the charge ratio asymptotically approaches the true value. However, the number of muons with $|\alpha| > \alpha_c$ available to determine the charge ratio also decreases. In Table III we show values of the average charge ratio computed by this orthodox method and the precent of dilution for various α_c. It is obvious that it is not practical to simply increase α_c, as the standard deviations would become so large as to make the results meaningless. Therefore, a compromise is made in the choice of α_c to include the maximum number of muons without excessive dilution in the charge ratio. How much dilution remains in the charge ratio for a given α_c is difficult to reliably estimate, and all previous attempts have given values

TABLE I. Results of least-squares charge-ratio analysis. N =number of muons; h =mean slant depth (10^2 g cm^{-2}); θ =mean zenith angle; $|\phi|$ =mean azimuth angle; E_μ =mean muon energy at production (GeV); R_0 =charge ratio; w_0 =width parameter; χ_ν^2 =reduced χ^2; $\langle R_0 \rangle = 1.378 \pm 0.015$.

Bin	N	h	θ	$|\phi|$	E_μ	R_0	w_0	χ_ν^2
1	242 90	2524.66	46.46	2.74	1004	1.402 ± 0.034	0.827 ± 0.012	1.90
2	347 50	2744.97	54.40	4.51	1137	1.372 ± 0.028	0.954 ± 0.011	0.99
3	192 24	3283.28	56.05	2.59	1500	1.351 ± 0.038	0.940 ± 0.013	0.84
4	317 29	3393.99	63.41	3.79	1583	1.384 ± 0.031	0.960 ± 0.010	0.51
5	6505	4350.45	66.61	5.42	2429	1.367 ± 0.071	0.938 ± 0.022	0.51
6	3899	4404.85	72.23	12.26	2488	1.362 ± 0.093	0.905 ± 0.026	0.82
7	408	5356.66	67.54	14.90	3626	1.765 ± 0.400	0.985 ± 0.095	0.87
8	2572	5386.07	74.83	3.49	3675	1.404 ± 0.121	0.933 ± 0.034	0.64
9	1920	6326.31	77.23	17.02	5191	1.289 ± 0.194	0.578 ± 0.020	1.02
10	825	7385.45	77.82	18.37	7456	1.573 ± 0.304	0.595 ± 0.030	1.08

that were too small by at least a factor of two. Therefore, this orthodox method was abandoned in favor of a least-squares fitting procedure free of this problem.

V. DISCUSSION OF ERRORS

A. Bending-angle resolution-function error

In our least-squares charge-ratio analysis, we have assumed that the bending-angle resolution function for the magnets $B(\alpha, w_0)$ is approximately related to that for the concrete absorber $B_a(\alpha)$ via Eq. (11). To estimate the error we make in the charge ratio as a result of this assumption, we have chosen two different functions for $B(\alpha, w_0)$. The least-squares analysis was then performed for both functions, and the charge in the resulting charge ratio and χ^2 observed. The data of bin 2 were used in the fits because the small standard deviation of R_0 provided the most sensitive test.

The functions chosen were a Gaussian and a Lorentzian[21] distribution. The standard deviation of the Gaussian distribution and the half width at half maximum of the Lorentzian were allowed to vary as free parameters in the least-squares fit. The reduced χ^2 for 46 degrees of freedom was

TABLE II. Final charge-ratio results. For definitions of quantities, see caption of Table I.

h	θ	E_μ	R_0
2658	51.27	1084	1.384 ± 0.022
3349	60.44	1549	1.371 ± 0.024
4370	68.66	3451	1.365 ± 0.056
5384	74.22	3671	1.434 ± 0.116
6326	77.23	5191	1.289 ± 0.194
7385	77.82	7456	1.573 ± 0.304

7.96 for the Gaussian and 10.92 for the Lorentzian distribution. The charge-ratio values were 1.345 ± 0.026 and 1.377 ± 0.028, respectively. The rms deviation for the Gaussian distribution and half width at half maximum for the Lorentzian distribution had values of 5.4 ± 0.1 mrad and 2.8 ± 0.1 mrad. In Fig. 6 these distributions are shown with $B_a(\alpha)$ for comparison. Note that although the Gaussian and Lorentzian distributions are widely different, the discrepancy of the two resulting charge ratios is only on the order of one standard deviation in R_0 of bin 2. Thus, the determination of the charge ratio is not very sensitive to the choice of the resolution function as long as it conforms to the general shape of $B_a(\alpha)$.
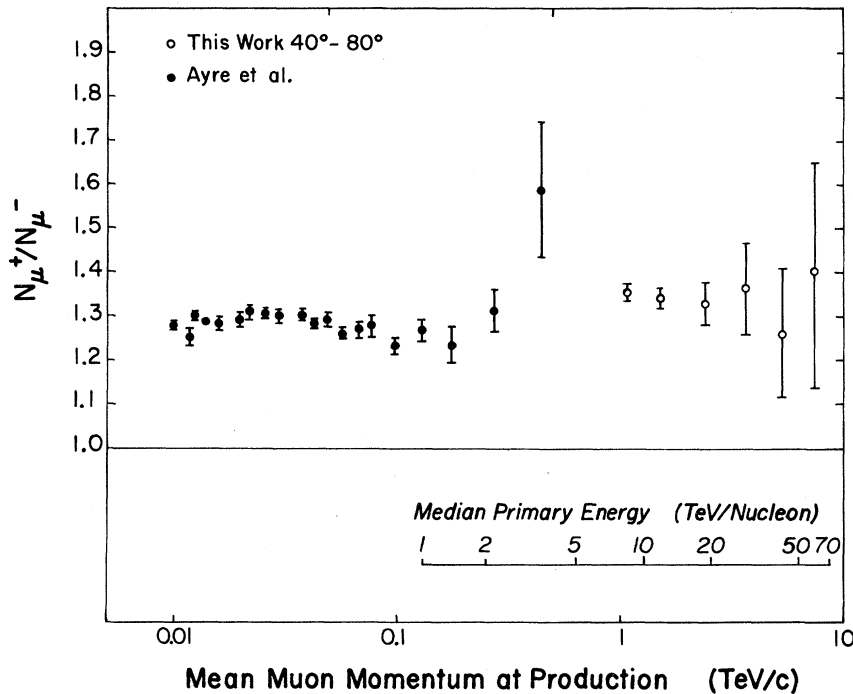

FIG. 8. The Utah charge-ratio measurements compared with the vertical measurements of Ayre *et al.* Our points are at mean zenith angles 51°, 60°, 69°, 74°, 77°, and 78°, which increase with energy.

B. Vertical depth-intensity error

Knowledge of the ideal bending-angle spectrum $j(\alpha_B, R_0)$ to within the value for the charge ratio R_0 is tantamount to a knowledge of the vertical depth-intensity spectrum $I_v(x)$. By fitting Miyake's form for the vertical depth-intensity spectrum,[22]

$$I_v(x) = Ae^{-x/\lambda}x^{-s}(x+x_0)^{-1} , \qquad (14)$$

to the data between 10^5 g cm^{-2} and 10^6 g cm^{-2}, and then proceeding with the analysis for the charge ratio, we can see how sensitive R_0 is to the choice for $I_v(x)$. The Miyake vertical depth-intensity spectrum is enough different from Eq. (4), while still giving a reasonable fit to the data, to provide a good indication of the sensitivity in R_0. Again, the least-squares fit was made to the data of bin 2 for the best test.

The results of the fit were $R_0 = 1.375 \pm 0.026$, $w_0 = 0.985 \pm 0.012$, and $\chi_v^2 = 0.90$. The discrepancy between this value for the charge ratio and that of bin 2 is about $\frac{1}{2}$ of a standard deviation. The reduced χ^2 is slightly better using the Miyake spectrum; however, the Miyake spectrum does not fit the vertical depth-intensity data as well as Eq. (4), the reduced χ^2's being 1.22 and 1.00, respectively, for 10 degrees of freedom. Therefore, we prefer our choice of Eq. (4) for the vertical depth-intensity spectrum over our range of slant depths.

When comparing Eq. (4) with a later and more sophisticated least-squares fit by Groom[23] to a world survey of vertical depth-intensity data, the discrepancy between the two spectra as a function of depth is mirrored by the variation of χ_v^2 with h in Table I. This we interpret as a combination of agreement of Eq. (4) with the true vertical depth-intensity spectrum and big statistical errors at large slant depths.

C. Asymmetric muon energy loss error

Because all muons in this charge-ratio experiment traversed at least 781 m of rock before reaching the detector, we investigated the effects of the asymmetric rates of energy loss for μ^+ and μ^- upon the charge ratio. The validity of quantum electrodynamics was assumed to obtain an estimate of the size of the asymmetry. This estimate was compared with experimental values where available. From the respective rates of energy loss, the energies E^+ and E^- for μ^+ and μ^- to stop at a slant depth x were computed assuming continuous energy losses. The ratio of the charge ratio at depth x, $R(x)$, to the charge ratio at the surface R_0 is then just the ratio of the number of μ^+ to the number of μ^- at the surface with the respective energies E^+ and E^-. The effect of the asymmetry in the energy loss rates was examined

TABLE III. Average value of the charge ratio for muons with $|\alpha| > \alpha_c$, and percent of reduction from the average least-squares result 1.378.

α_c	R	% dilution
0	1.160 ± 0.007	15.8 ± 1.0
8	1.260 ± 0.012	8.6 ± 1.3
14	1.294 ± 0.018	6.1 ± 1.7
20	1.299 ± 0.024	5.7 ± 2.0
30	1.365 ± 0.038	1.0 ± 3.0

separately for ionization and for bremsstrahlung and pair production.

Ionization. If the μ-e scattering amplitude is expanded to include higher-order terms in e^2, a difference in the cross section for μ^-e^- and μ^+e^- results. To order e^6 this is due to interference between amplitudes for one- and two-photon exchange. By applying an expansion of the Mott scattering formula to include terms in e^6, Jackson and McCarthy[24] have evaluated corrections to the stopping power of μ^+ and μ^-. The energy-loss formula to this order in e^2 can be written

$$-dE/dx = z^2 I + z^3 J , \qquad (15)$$

where z is the sign of the muon charge. For $2 < p/Mc < 20$, they report that J is approximately constant and causes a range difference $\Delta x = x^+ - x^-$, which is roughly proportional to the mean range x for stopping particles of the same mass and energy, but has opposite charge. The change in $\Delta x/x$ is less than -0.3% for muon momentum greater 0.1 GeV/c, and depends only slightly on the stopping material, varying from -1.9×10^{-3} for carbon to -2.5×10^{-3} for lead with $z = \pm 1$. The results of Jackson and McCarthy are in good agreement with measurements by Clark *et al.*[25] for positive and negative muons with initial momenta between 0.015 and 1.6 GeV/c. Assuming $\Delta x/x < -2.5 \times 10^{-3}$ and that energy loss terms are constant, we estimate that $R(x)/R_0 > -0.993$. This is less than about $\frac{1}{2}$ a standard deviation of the charge-ratio values listed in Table I.

Bremsstrahlung and pair production. The contribution to bremsstrahlung from collisions of a muon and atomic electrons is important for materials of low atomic number Z such as the rock overburden of the detector. To lowest order, μ-e bremsstrahlung consists of four Feynman diagrams. These diagrams can be classified as follows: type A, the photon is emitted by the muon, and type B, the photon is emitted from the electron. The contribution of diagrams A is similar to μ-photon bremsstrahlung.[26] The interference of diagrams A and B has opposite signs for μ^+ and μ^-, and therefore gives rise to an asymmetric

energy loss. In evaluating the cross section for relativistic e^+e^- bremsstrahlung, Swanson[27] observes that the square of the matrix element is dominated by the regions where the propagator denominators are near a pole. Thus, we expect the pole regions also to dominate in the μ-e bremsstrahlung because of the similarity to the e^+e^- case. Since the poles are kinematically separated, there will be negligible contribution from the interference of diagrams A and B. Physically, the radiation is emitted in cones about the direction of the muon and electron momenta. At large muon energies, the opening angles of these cones is small. Thus, there will be little overlap between the two cones resulting in almost no interference contribution. Altarelli and Buccella[28] obtain an upper bound for the interference cross section in e^+e^- bremsstrahlung by relating it to the noninterference cross sections via the Schwarz inequality. We make a rough estimate of the μ-e interference cross section following their method— except that we use the muon mass in terms which correspond to muon propagators, and the cross sections given by Rozental[29] for the contributions of diagrams A and B. The result we obtain is that the interference cross section varies with muon energy approximately as $E^{-3/2}$.

We assume the asymmetric energy loss for pair production is of the same order as for bremsstrahlung because of the similarity in their respective Feynman diagrams, and write the energy-loss formula as

$$- dE/dx \sim a + bE - zb\xi_0 E^{-1/2} , \qquad (16)$$

where $a \sim 2.8$ MeV/g cm^{-2}, $b \sim 4 \times 10^{-6}$ g^{-1} cm^2, and $\xi_0 \lesssim 0.93$ GeV$^{3/2}$. Thus, we estimate that $R(x)/R_0 \lesssim 1.003$. This corresponds to a change in the charge ratio of less than 20% of one standard deviation in Table I, and of less than $\frac{1}{2}$ of that due to an asymmetry in the ionization energy loss.

D. Systematic bending-angle correction error

If an error is made in determining the systematic bending-angle error α_s, the two histograms for a given muon direction will not be brought into coincidence, and the resulting total histogram will be broadened. We investigate the effect of this broadening on the charge ratio as follows. Two histograms identical to that of bin 2 are constructed. We displace one by a specified bending angle $+\Delta\alpha$, and the other by $-\Delta\alpha$. The histograms are then averaged together so as to form a single histogram with a total number of muons equal to that of bin 2. We then determine the charge ratio via our least-squares analysis. For

$\Delta\alpha = 2$ and 4 mrad, we obtain the results in Table IV. The largest statistical error for α_s is less than $\frac{3}{4}$ mrad; therefore, the enhancement for the charge ratio is less than about 0.05%. The fact that we have equal numbers of muons in each of the two histograms guarantees that the effect on the charge ratio will be small. For this reason the magnetic induction field was reversed at the proper times to give nearly equal numbers of muons in each histogram for a given muon direction.

VI. DISCUSSION

The Utah charge-ratio results extend about a decade in muon energy beyond other currently existing measurements. The comparison in Fig. 8 of our results from Table II with the vertical measurements of Ayre et al.[2] depicts the general behavior of the charge ratio over three decades of muon energy starting at 10 GeV. The results of Ayre et al. were chosen as representative of the many fine low-energy measurements.[1-6] This three-decade range of muon energy converts to a median primary energy range from 78 GeV/nucleon to 58 TeV/nucleon. The equivalent laboratory energy range of the CERN ISR is from 63 GeV to 2 TeV. Thus, the charge ratio is fairly well determined over an energy range extending not only over the ISR range of laboratory energies, but well beyond.

Critical to the interpretation of the charge ratio is an understanding of the composition of the primary cosmic-ray spectrum, the dynamics of the hadronic interactions ("hadrodynamics"), and, to a lesser degree, the spectral slope(s) of the primaries. Until about the start of this decade, knowledge of the primary composition and slope was assumed to be less uncertain than that of the hadronic interactions. Thus the charge-ratio measurements were used to provide a constraint on models of the hadronic interactions,[30] assuming that the composition and slope remained constant.[31]

With the extension of accelerator energy into the lower cosmic-ray range via the ISR, the pos-

TABLE IV. Charge ratio R and percentage error as a function of the error in the systematic bending-angle error correction for bin 2. $w(\Delta\alpha_s)$ is inversely proportional to the width of the bending-angle resolution function.

$\Delta\alpha_s$ (mrad)	$R(\Delta\alpha_s)$	$\Delta R/R(0)$ (%)	$w(\Delta\alpha_s)$
0	1.372 ± 0.028	0	0.954 ± 0.011
2	1.374 ± 0.029	0.13	0.876 ± 0.009
4	1.390 ± 0.030	1.30	0.721 ± 0.007

sibility arose of utilizing the scaling/limiting-frag-mentation hypothesis[32-34] to determine the hadron-ic interaction dynamics.[35] Basically, this hypothe-sis refers to the asymptotic energy independence of the *inclusive* distribution. A single-particle inclusive reaction is one in which measurements of other produced particles are excluded; e.g., $p + p \rightarrow \pi +$ anything. Although the concept of the scaling-limiting-fragmentation hypothesis is not new to cosmic-ray physics,[36] it is more precisely defined by the new accelerator data. This hypothe-sis together with assumptions about the composi-tion and spectral slope of the primaries has been used to make charge-ratio predictions to test the over-all validity of the model, or scaling-limiting-fragmentation has been assumed and the charge ratio used to infer the behavior of the primary composition. However, recently small deviations from this hypothesis have been observed in the data.[37] But taken as a first approximation, the agreement between the charge-ratio predictions by various workers and the experimental results is not too bad. For example, the combination of Feynman scaling[32] with a constant primary slope and composition qualitatively agrees with the in-crease of the charge ratio with muon energy due to increased kaon production.[10] A survey of the current situation of charge-ratio predictions is given by Erlykin, Ng, and Wolfendale.[38] The range of the listed predictions is mainly the re-sult of differing fits to accelerator data.

Since the charge ratio depends upon the differ-ence between positive and negative meson produc-tion, it is very sensitive to the dynamics of the hadronic interactions— more so than the sea-level muon intensity, for example. The charge ratio is well known over a wide energy range. The mea-surements have become fairly precise, and most of them are in agreement. Therefore, we believe the charge ratio will continue to serve as a valu-able touchstone in determining the hadronic inter-action dynamics and composition of the primary cosmic rays.

ACKNOWLEDGMENTS

*Research supported by the National Science Foundation.

†This paper forms the thesis submitted to the University of Utah in partial fulfillment of the requirements for the Ph.D. degree.

‡Present address: Bechtel Corp., Nuclear Power Division, Box 3965, 50 Beale Street, San Francisco, California 94119.

§Deceased.

‖Present address: Lawrence Livermore Lab, P. O. Box 808, Livermore, California 94550.

[1]M. G. Thompson, in *Cosmic Rays at Ground Level*, edited by A. W. Wolfendale (International Scholarty Book Service, Portland, 1974), pp. 44–48.

[2]C. A. Ayre *et al.*, in *Proceedings of the Thirteenth International Conference on Cosmic Rays, Denver, 1973* (Colorado Associated Univ. Press, Boulder, 1973), Vol. 3, p. 1822.

[3]O. C. Allkofer *et al.*, in *Proceedings of the Twelfth International Conference on Cosmic Rays, Hobart, 1971*, edited by A. G. Fenton and K. B. Fenton (Univ. of Tasmania Press, Hobart, Tasmania, 1971), Vol. 4, p. 1319.

[4]B. C. Nandi and M. S. Sinha, Nucl. Phys. B40, 289 (1972).

[5]T. H. Burnett *et al.*, Phys. Rev. Lett. 30, 937 (1973).

[6]T. H. Burnett *et al.*, in *Proceedings of the Thirteenth International Conference on Cosmic Rays, Denver, 1973* (Ref. 2), Vol. 3, p. 1764.

[7]G. W. Carlson, Ph.D. thesis, Univ. of Utah, 1973 (un-published).

[8]J. H. Parker, Ph.D. thesis, Univ. of Utah, 1969 (un-published).

[9]G. K. Ashley, II, J. W. Keuffel, and M. O. Larson, in *Proceedings of the Thirteenth International Conference on Cosmic Rays, Denver, 1973* (Ref. 2), Vol. 3, p. 1828.

[10]G. K. Ashley, II, *et al.*, Phys. Rev. Lett. 31, 1091 (1973).

[11]J. W. Keuffel and J. L. Parker, Nucl. Instrum. Methods 51, 29 (1967).

[12]L. K. Hilton, M. L. Morris, and R. O. Stenerson, Nucl. Instrum. Methods 51, 43 (1967).

[13]H. E. Bergeson and C. J. Wolfson, Nucl. Instrum. Methods 51, 47 (1967).

[14]G. L. Cassiday, D. E. Groom, and M. O. Larson, Nucl. Instrum. Methods 107, 509 (1973).

[15]B. Rossi, *High-Energy Particles* (Prentice-Hall, New Jersey, 1952), p. 16.

[16]B. Rossi, *High-Energy Particles* (Ref. 5), p. 14.

[17]K. U. Wilson, M. S. thesis, Univ. of Utah, 1972 (unpub-lished).

[18]D. E. Groom, Univ. Utah Cosmic-Ray Group Internal Note No. UUCR-102 (unpublished).

[19]G. W. Carlson and J. L. Morrison, Univ. of Utah Cosmic-Ray Group Internal Note No. UUCR-118 (un-published).

[20]P. R. Bevington, *Data Reduction and Error Analysis for the Physical Sciences* (McGraw-Hill, New York, 1969), pp. 243–245.

[21]P. R. Bevington, *Data Reduction and Error Analysis for the Physical Sciences* (Ref. 20), pp. 49–53.

[22]S. Miyake, V. S. Narashimham, and P. V. Ramana Murthy, Nuovo Cimento 32, 1505 (1964).

[23]D. E. Groom, private communication.

[24]J. D. Jackson and R. L. McCarthy, Phys. Rev. B $\underline{6}$, 4131 (1972).

[25]A. R. Clark et al., Phys. Lett. $\underline{41B}$, 229 (1972).

[26]V. M. Galitskii and S. R. Kelner, Zh. Eksp. Teor. Fiz. $\underline{52}$, 1427 (1967) [Sov. Phys.—JETP $\underline{25}$, 948 (1967)].

[27]S. M. Swanson, Phys. Rev. $\underline{154}$, 1601 (1967).

[28]G. Altarelli and F. Buccella, Nuovo Cimento $\underline{33}$, 115 (1964).

[29]I. L. Rozental, Usp. Fiz. Nauk $\underline{94}$, 91 (1968) [Sov. Phys.—Usp. $\underline{11}$, 49 (1968)].

[30]M. G. Thompson, in Cosmic Rays at Ground Level, edited by A. W. Wolfendale (Ref. 1), pp. 48–53.

[31]M. Garcia-Munoz, in Proceedings of the Thirteenth International Conference on Cosmic Rays, Denver, 1973 (Ref. 2), Vol. 5, p. 3513; J. F. Ormes et al., ibid., Vol. 1, p. 157.

[32]R. P. Feynman, Phys. Rev. Lett. $\underline{23}$, 1415 (1969).

[33]J. Benecke et al., Phys. Rev. $\underline{188}$, 2159 (1969).

[34]W. R. Frazer et al., Rev. Mod. Phys. $\underline{44}$, 284 (1972).

[35]N. F. Bali et al., Phys. Rev. Lett. $\underline{25}$, 557 (1970).

[36]E. L. Feinberg, Phys. Rep. $\underline{5C}$, 240 (1972).

[37]W. R. Frazer, in Proceedings of the Thirteenth International Conference on Cosmic Rays, Denver, 1973 (Ref. 2), Vol. 5, p. 3354.

[38]A. D. Erlykin, L. K. Ng, and A. W. Wolfendale, J. Phys. A $\underline{7}$, 2059 (1974).